Effect of Non-invasive Spinal Stimulation on Self-sustained Firing Motoneuron Model: In-Silico Study Using Human Body Model

Hyungtaek Kim, Cheolki Lim, Jong Seung Lee, Donghyeon Kim, Chae-Bin Song, and Yasin Dhaher

***Abstract*— Transcutaneous spinal electrical stimulation (tSCS) is a non-invasive neuromodulation approach using a low intensity direct current. Recent developments in the technique have opened the possibility that tSCS can help restore motor function after spinal cord injury (SCI). However, the exact mechanism of action tSCS has on the spinal circuits is still unknown. Due to the complexity of experimental synthesis in a human model to delineate the mechanisms, models that link the stimulation paradigm and circuit behaviors are advantageous. Thus, this study aims to simulate the underlying changes in motor circuit firing rates in response to external stimuli induced by tSCS. Serial stimulations combining a high-fidelity finite element model with the human torso and spinal cord with a lumped motor neuron model is constructed. The parameters for both components of the model were derived from previous studies. We focused our analysis on a lumped motor neuron model that describes sustained firing behavior of the motor neuron driven primarily by persistent inward current (PIC), a signature behavior of the motor neuron after SCI. Modulation of the PIC behaviors was achieved by stimulating voltage-dependent calcium and sodium channels in the dendrite using a tSCS-induced electric field (E-field) expressed at different a spatial locations of the motor neuron in the gray matter. The PIC behaviors of spinal motor neurons in the left ventral horn were suppressed, while for the most part invariant in the right ventral horn. These initial simulations will provide a steppingstone for future examinations that incorporate additional neuronal models of inhibitory and excitatory interneurons to access the circuit-level effect of spinal stimulation.**

I. Introduction

In recent years, several examinations have shown that electrical stimulation of the spine can induce changes in the excitability of the spinal circuit in animals and humans [1], [2]. Furthermore, recent technological advances have opened the possibility that tSCS can help to regain some of the motor functions lost after SCI [3]. However, the observed effects of these stimulations varied across subjects with no mechanistic interpretations of the origins of the observed variability. Previous studies suggested that variations in conductivities and volume of tissue layers could result in significant changes in the induced E-field across subjects [4]. Thus, we created a high-fidelity human body model from tissue-labeled MR images containing segments of the tissue layers. The goal is to construct an in-silico simulation platform to estimate tSCS-induced E-field more precisely, considering the human body's complex anatomical structures and tissue layers' varying conductivities.

To assess the manifestation of of tSCS-induced E-field simulation on the excitability of spinal circuits, we coupled the aggregate results with a simplified model of a motor neuron experiencing prolonged firing activity, a persistent inward current-driven activity (PIC). It has been proposed that PIC is a phenomenon that induces sustained firing in SCI due to loss of inhibitory control after injury[3]. Accordingly, we employed a two-compartment lumped neuron model to simulate the PIC-induced sustained firing of motor neurons. Prior studies suggest that voltage-dependent calcium and

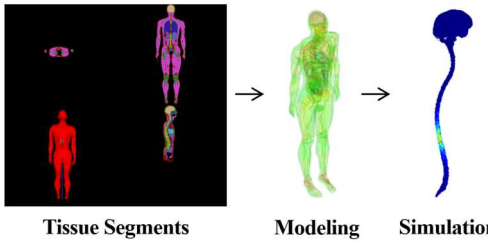

Fig 1. Representative images of each step of human modelling creation and tSCS simulation pipeline.

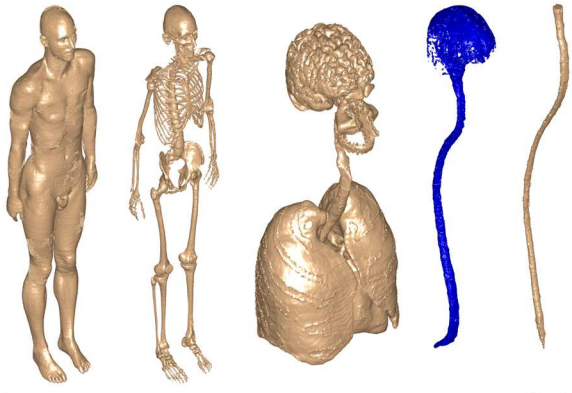

Electrical Conductivity

Layer	Name	σ values	Ref	Layer	Name	σ values	Ref
1	Skin	0.435	[3]	7	Spinal Cord	0.532	[3]
2	Bone	0.06	[3]	8	Visceral	0.123	[4]
3	Lungs	0.046	[3]	9	Brain	0.29	[4]
4	CSF	1.79	[3]	10	Cartilage	0.18	[4]
5	Heart	0.535	[3]	11	Electrode	2.00E-02	[3]
6	Muscle	0.355	[3]				

Fig 2. Tissue layers of the body model and corresponding isotropic electrical conductivities

Hyungtaek Kim is with Neurophet Inc, Seoul, South Korea, on leave from the University of Texas Southwestern Medical Center, Dallas, Texas (e-mail: Hyungtaek.Kim@UTsouthwestern.edu).

Cheolki Im is with School of Electrical Engineering and Computer Science, Gwangju, Institute of Science and Technology, Gwangju, 61005, South Korea.

Jongseong Lee, Donghyeon Kim and Chae-bin Song are with Neurophet Inc, Seoul, Gangnam-gu, Taheran-ro, 124, South Korea

Yasin Y. Dhaher is with University of Texas Southwestern Medical Center, Dallas, Texas (e-mail: Yasin.Dhaher@UTSouthwestern.edu)

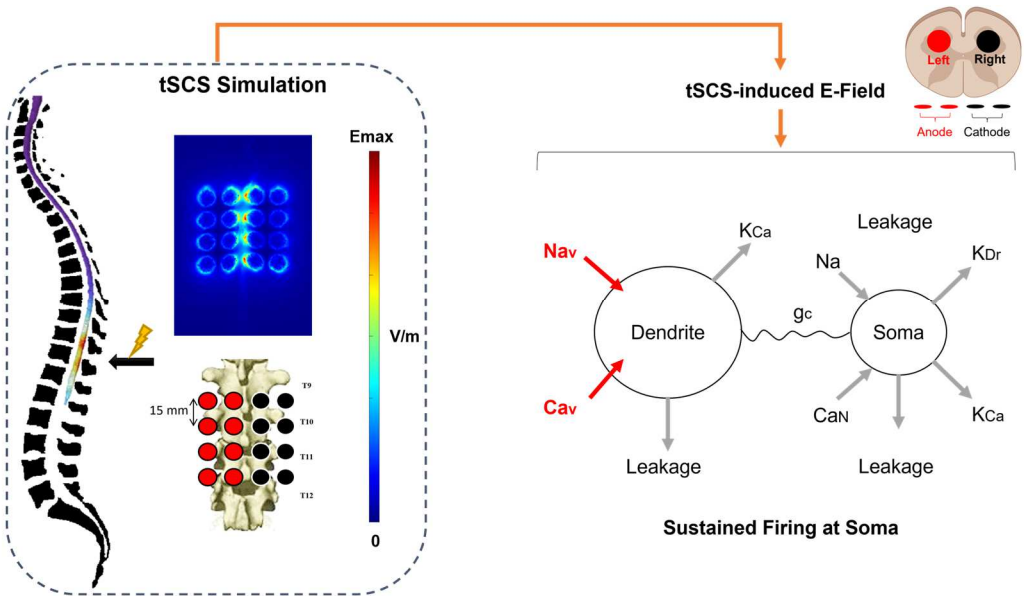

Fig 3. Schematics of the tSCS-induced E-field (input) by a multi-electrode array to voltage-dependent channels (Na_v and Ca_v) in a PIC-spinal neuron model. Black circles represent the cathode, and red circles represent the anode. The cross-sectional rendering of the cord in the figure shows locations where the average E-field induced by the grid is calculated. The simulation of the PIC circuit shown on the left and right of the figure was repeated. Note that the E-field on the right and the left are different in not only the field direction but the amplitude due to the multilayer isotropic analysis employed by the FEM.

sodium channels in the dendrite could be targets for tSCS to modulate PIC behaviors [11]. Consequently, we tried to modulate the behaviors of sustained firing by employing a tSCS-induced E-field on these voltage-dependent channels.

In the present study, we propose a pipeline of silico simulations that estimate the E-field during tSCS across spinal segments and the impact of the estimated E-field on the spinal circuits. The goal is to develop the first step of an in-silico simulation pipeline that can potentially conduct future examinations on the design of transcutaneous spinal cord stimulation paradigms.

II. Method

A. Human Model

To estimate the stimulation-induced effect on human spinal columns, we constructed a volumetric mesh model using the 34-year-old Duke male model of the Virtual Population Family[4]. The surface meshes of 22 tissue masks from the model were converted into binary image files and merged into 11 layers (Fig. 2). The layer containing the stimulation electrodes was manually identified. The multi-electrode montages with 16 circular electrodes (15 mm in diameter) placed in a 4x4 grid were used in this study. The montage was placed in the center of T10, midway between the spinous processes of vertebrae T9 and T11. Binary images of each layer were assembled, and volume mesh generation was performed using CGAL version 4.0. CGAL enabled the conversion of segmented magnetic resonance data into a 3D tetrahedral mesh. An electrical conductivity of 0.02 S/m was assigned to the electrode, derived from the material properties of the hydrogel [4].

B. Finite element model (FEM)

After mesh generation, the tSCS problem was defined by transforming a stereotypical format of Maxwell's equation to satisfy the parameters of the tSCS conditions.

$$\nabla \cdot \nabla V = 0 \; in \; \Omega \quad \text{Eqn (1)}$$

V is the potential induced by the inward current applied by tSCS, and Ω is the domain defined by the human body model. The equation satisfies the insulation condition in most outer boundaries when the inner product between the normal vector and the current density equals zero. Equation (1) was solved using the finite element method, and the Eigen library was used as a solver to compute the tSCS-induced E-field with the conjugate gradient (CG) method.

C. Electrical Stimulation (FEM model input)

For this study, we employed a multi-electrode array stimulation system applied transcutaneously on the spine. Grid stimulation consisted of a 4x4 set of electrodes split in half for the anode and cathodes. Our stimulation intensity was

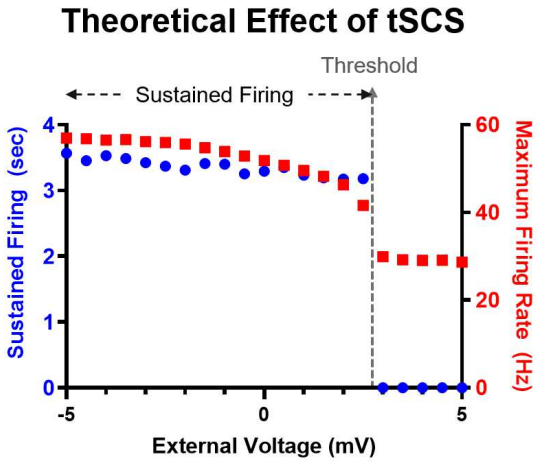

Fig 4. The theoretical effect of tSCS corresponding to external stimuli ranged from -5 to 5 mV. The time of the sustained firing of the soma (blue) and the maximum firing rate was illustrated (red).

limited to a 5 mA pair of electrodes, a total of 40 mA stimulation was used. The safety considerations of using a multi-electrode montage in this study should be addressed. The estimated maximum current density on the skin and spinal cord ranged from 8.02 to 29.42 A/m^2. The maximum current density was generated near the skin-to-electrode interface when stimulating 5 mA. Considering that 143 A/m^2 is a threshold for tissue/nerve damage[5], 29.42 A/m^2 was below the threshold; therefore, the montage and parameter used in this study may be safe.

D. *Two*-compartment *Pic spinal motoneuron model*

This paper's lumped neuron model consists of two coupled compartments representing dendrite and soma. All parameters of the coupled model were derived from Kurian et al.[6]. Kurian et al. indicated that persistent firing was achieved when the coupling conductance (g_c) and the ratio of the somatic surface area to the total surface area (p) were set at 0.1. The neuron model was numerically simulated using the ode15s solver in MATLAB (MathWorks, Natick, United States). The duration of sustained firing, the total firing time, and the firing frequency were determined following the definitions of Kurian et al. [6]. A total firing duration below 5 s was considered normal, a state of normal firing was not observed.

E. *Serial Simulation*

We calculated the average E-field in the two areas of the cord relative to the center of the spine, the left and right ventral horns, as shown in the inset of Fig. 3 The resulting tSCS-induced E-field at both locations were as an input stimulus to the two-compartment spinal cord neuron model (Fig. 3). The input voltage was converted from the E-field using an average diameter of the alpha motor neuron reported by [7]. In the serial stimulation, we wanted to test if the exposure of the PIC-producing lump model can be perturbed by superimposing finite element-induced E-field. Specifically, we wanted to test whether the spatial location of the motor neuron, the left or right ventral horn, will have a different effect on the PIC behavior of the motor neuron. To implement this effect, a lumped model with parameters expressing the PIC behavior was initially simulated with an external voltage as the input at time 0.

III. RESULT

A. *Theoretical effect of tSCS*

We generated a theoretical response of the PIC circuit model relative to a set of input stimulation intensities ranging from 0 to 5 mA (Fig. 4). Modulation by the negative voltage marginally increased the duration of sustained firing and the firing rates. On the other hand, positive voltage inhibited sustained firing. At the threshold (3.0 mV), sustained firing was not observed, and the firing rate was unchanged.

B. *Effect of tSCS*

A representative figure indicated that the duration of the sustained firing of a motor neuron could be modulated in both the left and right ventral horns. The observed tSCS-induced modulation was marginal but excitatory in the right ventral horn. On the contrary, sustained firing was suppressed in the left ventral horn (Fig. 5), and at least five mA is necessary to induce the observed inhibitory effect (Fig. 6).

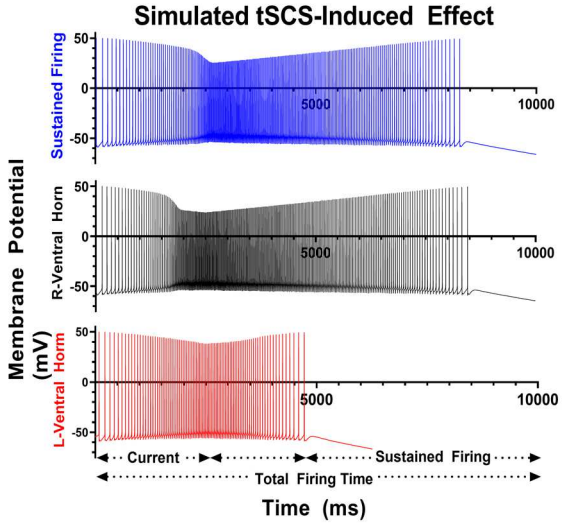

Fig 5. Effect of tSCS-induced E-field in PIC-employed spinal motor neuron model. Note that changes in motor unit firing patterns in left ventral horn (red), right ventral horn (black) and PIC producing lump model (blue) were compared. External stimuli (mV) were estimated from the body model.

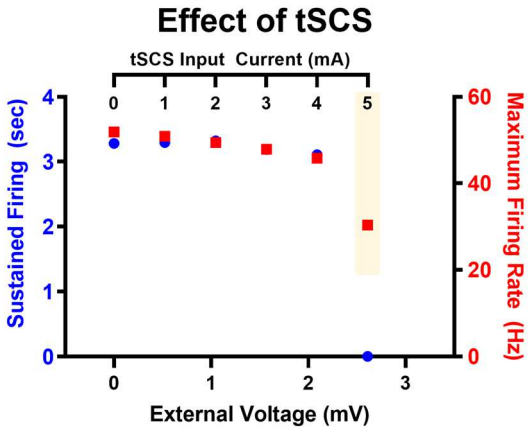

Fig 6. Effect of tSCS in left ventral horn; input stimulation current ranged from 0 to 5 mA. At 5mA (yellow), the average voltage at the target spinal cord was near the threshold.

IV. DISCUSSION

Our main goal was to establish a computational framework that links transcutaneously applied electrical stimulation with motor neuron firing properties. This framework combined a high-fidelity finite element model and a lumped neuronal model of the spinal motor neuron. We sought to establish that transcutaneous stimuli will produce a neuromodulatory effect on motor neurons. This effect would likely be sensitive to the spatial location of the motor neuron in the spinal cord.

Prior studies showed that the varying conductivities and volume of the tissue layers could result in significant variability in the induced E-field [4]. Our FEM considers both complexities and thus, we argue that the in-silico simulation employed herein provides a more realistic estimation of the

E-field. Hence, the effect observed is likely due to the spatial-neuronal characteristics of the spinal circuit.

The inhibitory effect induced by a positive voltage in the left ventral horn was consistent with the findings of anodal transcutaneous stimulation studies indicating stimulation-induced inhibition [8]. On the other hand, transcutaneous cathodal spinal stimulation has been reported to produce up-regulation of motor neuronal excitability [9], [10]. Our simulation shows a slight increase in sustained motor neuronal activity in the right ventral horn. These results indicate that a grid-like stimulation paradigm simulated in this study will likely have a clear unilateral effect, in the case of inhibition, rather than a bilateral effect. However, these simulation results are likely affected by the assumptions of the two-compartment model that do not incorporate the 3-dimensional morphological representation of motor neurons [8].

We used the PIC-induced spinal circuit, a widely supported mechanism of sustained muscle activation in SCI. Prior studies indicated that the inhibitory stimulation-induced effect by the spinal cord stimulation could attenuate PIC-induced sustained firing. However, the mechanisms underlying the observed inhibition remain unclear. Here, our computational pipeline may provide some insight into understanding potential tSCS-induced effects in the behavior of PIC-embedded spinal circuitry.

We generated volume mesh using a binary magnetic resonance image, a widely accepted technique in in-silico tDCS studies. The main bottleneck to applying this technique in the human spinal cord is the lack of a precise segmentation tool to represent the spinal cord and other surrounding tissues. The spinal cord toolbox (SCT) offers spinal cord segmentation by creating a probability map of the spinal segments. However, the tool only creates labels for the cord and vertebrae;[11] . Therefore, a more advanced technique is required to estimate the effects induced by transcutaneous spinal stimulation. Thus, the advanced segmentation technique will allow subject-specific estimation of tSCS effect using the subject's MRI.

It is worth noting that many parameters were used on the high-fidelity FEM and motor neuron models. either. Some of the parameters are experimentally proven, and other parameters are based on the prior assumptions. A future examination should explore large-scale sensitivity analysis to apportion the effect of the given parameters either on the lumped motor neuron model or FEM in the context of excitability of the motor neuron, in this case, the sustained firing pattern of motor neuron.

Although simple and cost-effective, the tSCS technique have shown multiple benefits in functional recovery after SCI [1]. However, there needs to be a significant knowledge gap in our understanding of the underlying mechanisms. Our lack of understanding of the mechanistic pathways hinders our ability to explain the significant experimental variability observed within and between subjects when spinal stimulation is used. The computational framework presented here can provide insight into the mechanisms or provide data to inform the design of future experimental studies.

ACKNOWLEDGMENT

The authors express deep appreciation to the research team at Neurophet Inc. for helping us design a spinal cord simulation model.

REFERENCES

[1] A. Tjølsen, B. Linderoth, K. Hole, J. Wallin, and A. Fiskå, "Spinal cord stimulation inhibits long-term potentiation of spinal wide dynamic range neurons," *Brain Res*, vol. 973, pp. 39–43, 2003, [Online]. Available: http://www.sciencedirect.com/science/article/pii/S0006899303025307

[2] M. Bączyk and P. Krutki, "In vivo intracellular recording of type-identified rat spinal motoneurons during trans-spinal direct current stimulation," *Journal of Visualized Experiments*, vol. 2020, no. 159, pp. 1–8, 2020, doi: 10.3791/61439.

[3] G. Sandrini, M. Serrao, P. Rossi, A. Romaniello, G. Cruccu, and J. C. Willer, "The lower limb flexion reflex in humans," *Prog Neurobiol*, vol. 77, no. 6, pp. 353–395, 2005, doi: 10.1016/j.pneurobio.2005.11.003.

[4] A. Christ *et al.*, "The Virtual Family - Development of surface-based anatomical models of two adults and two children for dosimetric simulations," *Phys Med Biol*, vol. 55, no. 2, 2010, doi: 10.1088/0031-9155/55/2/N01.

[5] F. Cogiamanian, M. Vergari, F. Pulecchi, S. Marceglia, and A. Priori, "Effect of spinal transcutaneous direct current stimulation on somatosensory evoked potentials in humans," *Clinical Neurophysiology*, 2008, doi: 10.1016/j.clinph.2008.07.249.

[6] M. Kurian, S. M. Crook, and R. Jung, "Motoneuron model of self-sustained firing after spinal cord injury," *J Comput Neurosci*, vol. 31, no. 3, pp. 625–645, 2011, doi: 10.1007/s10827-011-0324-1.

[7] M. R. Martin, K. W. T. Caddy, and T. J. Biscoe, "579 With 2 figures Numbers and diameters of motoneurons and myelinated axons in the facial nucleus and nerve of the albino rat," 1977.

[8] F. Cogiamanian *et al.*, "Transcutaneous spinal cord direct current stimulation inhibits the lower limb nociceptive flexion reflex in human beings," *Pain*, vol. 152, no. 2, pp. 370–375, 2011, doi: 10.1016/j.pain.2010.10.041.

[9] T. Bocci *et al.*, "Cathodal transcutaneous spinal direct current stimulation (tsDCS) improves motor unit recruitment in healthy subjects," *Neurosci Lett*, 2014, doi: 10.1016/j.neulet.2014.06.037.

[10] A. Lamontagne, J. Fung, B. J. McFadyen, and J. Faubert, "Modulation of walking speed by changing optic flow in persons with stroke," *J Neuroeng Rehabil*, vol. 4, 2007, doi: 10.1186/1743-0003-4-22.

[11] B. de Leener *et al.*, "SCT: Spinal Cord Toolbox, an open-source software for processing spinal cord MRI data," *Neuroimage*, vol. 145, pp. 24–43, Jan. 2017, doi: 10.1016/j.neuroimage.2016.10.009.